ACES Asian Chemical Editorial Society

DOI: 10.1002/asia.201701323

CHEMISTRY AN ASIAN JOURNAL Full Paper

Nanoaggregates

Near-Infrared-Emissive Amphiphilic BODIPY Assemblies Manipulated by Charge-Transfer Interaction: From Nanofibers to Nanorods and Nanodisks

Jia-Fu Yin,[a, b] Yi Hu,[c] Huan Wang,[a] Zhong Jin,[c] Yi Zhang,[b] and Gui-Chao Kuang*[a]

Abstract: A novel near-infrared (NIR)-emissive amphiphilic BODIPY derivative, BBDP, was successfully prepared and thoroughly characterized. The photophysical properties in various organic solvents and THF/H_2O mixtures with different fractions of water were investigated. BBDP self-assembled into nanofibers in a water environment owing to its amphiphilic properties. Through charge-transfer interactions, BBDP co-assembled with a perylene bisimide derivative, PBI, and a viologen derivative, MV, to generate two superamphiphiles. These two superamphiphiles were able to aggregate in water media at appropriate concentrations. The BBDP–PBI charge-transfer complex formed nanorods, whereas the BBDP–MV aggregates expressed a disk-like morphology. This research paves the way for us to manipulate the morphology of dye assemblies.

Introduction

Amphiphilic aggregates with well-defined architectures have drawn considerable attention in the past decades because of their potential application in nanotechnology, biochemistry, and materials science.[1–8] Among them, near-infrared (NIR)-emitting dye assemblies play an important role in the fields of nanomaterials and biomedicine.[9–15] Boron–dipyrromethene (BODIPY) derivatives are important dye molecules because of their excellent fluorescent properties with high quantum yields and outstanding light stability.[15–17] Furthermore, structural modification to BODIPY dyes can significantly alter their photophysical properties. NIR-emissive BODIPY derivatives can be achieved by extensive aromatic ring fusion or by aza-nitrogen introduction at the *meso* position.[18–25] Amphiphilic BODIPY derivatives with a hydrophobic planar aromatic ring and hydrophilic parts have the potential to aggregate in aqueous solutions, which results in the formation of versatile topological structures such as nanowires, nanotubes, nanoribbons, and so on.[26–30] These sophisticated topological morphologies are commonly attributed to the complicated molecular structures. However, few studies report tuning of amphiphilic NIR-emissive BODIPY derivative self-assemblies by noncovalent driving forces.

A charge-transfer interaction is a typical type of noncovalent force that occurs between electron-rich molecule and electron-poor molecule.[31–35] Superamphiphiles induced by charge-transfer interactions can be obtained by simply mixing the donors with the acceptors in a solvent.[36] In this regard, this strategy has an advantage in that complicated and tedious synthesis procedures can be avoided. Since Kim et al. introduced the concept of a host-stabilized charge-transfer self-assembly,[37] significant progresses have been made by Zhang and co-workers in the field of superamphiphile charge-transfer assemblies. Versatile nanostructures have been realized by the rational design of intermolecular charge-transfer interactions.[38–44] On the other hand, functional and responsive parts can be integrated into the target molecules by charge-transfer interactions, so that novel assemblies with definite and distinct shapes and functional groups can be obtained.[44] Owing to the rapid expansion of biomaterials and medicinal chemistry, an increasing number of NIR-emissive materials are urgently needed. We are particularly engrossed in utilizing the charge-transfer strategy to construct various nanoscopic architectures with NIR amphiphilic molecules.

To address the abovementioned consideration, a novel NIR-emissive BODIPY derivative, BBDP, was constructed. To realize the NIR emission, two pyrene units were attached to the BODIPY core to extend the conjugated architecture. Three oligo(ethylene glycol) (OEG) chains were introduced as hydrophil-

[a] J.-F. Yin, H. Wang, Prof. Dr. G.-C. Kuang
State Key Laboratory of Power Metallurgy
Department of Polymer Materials and Engineering
Central South University
Changsha, Hunan 410083 (China)
E-mail: gckuang@csu.edu.cn

[b] J.-F. Yin, Prof. Dr. Y. Zhang
College of Chemistry and Chemical Engineering Department
Central South University
Changsha, Hunan 410083 (China)

[c] Y. Hu, Prof. Dr. Z. Jin
Key Laboratory of Mesoscopic Chemistry of MOE
School of Chemistry and Chemical Engineering
Nanjing University
Nanjing, Jiangsu 210093 (China)

Supporting Information and the ORCID identification number(s) for the author(s) of this article can be found under: https://doi.org/10.1002/asia.201701323.

ic parts. This amphiphilic BODIPY derivative possessing both hydrophobic and hydrophilic units was able to self-assemble in aqueous solution. Pyrene moieties are typical electron-rich units that behave as electron donors to provide electrons to electron acceptors. Perylene bisimide derivatives (e.g., PBI) and viologen derivatives (e.g., MV) are well-reported electron-poor molecules in charge-transfer systems.[31] We hope to obtain two co-assembly complexes between BBDP and the above two acceptors by using charge-transfer interactions. Then, the obtained charge-transfer complexes could be assembled in water media to display distinct morphologies.

Results and Discussion

Photophysical properties and aggregation behavior of BBDP

BBDP was prepared according to the synthesis route outlined in Scheme 1. Formyl-modified OEG dendrons **1** followed a classic synthetic pathway to BODIPY derivatives to afford target molecule **2**.[45] Then, compound **2** underwent a Knoevenagel reaction with 1-pyrenecarboxaldehyde to generate the final BBDP product.[26] PBI and MV were obtained according to the literature.[46,47] More details about the synthesis processes and characterization data are described in the Experiment Section.

The photophysical properties of BBDP in various organic solvents were investigated by UV/Vis and fluorescence (FL) spectroscopy (Figure 1). As for the UV/Vis spectra, the absorption band located between $\lambda = 680$ and 710 nm and the shoulder at approximately $\lambda = 650$ nm were assigned to the S0–S1 transition of the delocalized π-conjugated core and vibrational structure, respectively. The emission band of BBDP was located in the NIR range on account of the extensive conjugated pyrene–BODIPY architecture. Besides, BBDP showed small Stokes shifts in various solvents (less than $\Delta\lambda = 30$ nm), which indicated that there were weak intramolecular donor–acceptor interactions in the ground state.[45] More information about the photophysical data of BBDP are summarized in Table S1 (Supporting Information).

Owing to its classic amphiphilic characteristics, BBDP could self-assemble into NIR-emissive supramolecular aggregates in aqueous solution because of hydrophobic interaction and π–π stacking interaction driving forces. UV/Vis and FL spectroscopy were employed to trace the aggregation behavior of BBDP in THF/H_2O mixtures with different fractions of water. The absorption intensity decreased sharply, and this was accompanied by a hypsochromic shift in the absorption wavelength if the fraction of water reached 80% (Figure 2a). At the same time, the fluorescent emission decreased gradually and was fully quenched after the further addition of water (Figure 2b). The fluorescence quenching effect was assigned to strong π–π stacking interactions of the bent-shaped rod building blocks and to the existence of hydrophobic interactions during the formation of the nanoaggregates.[30,48] The above evidence was sufficient to prove that the BBDP molecules form H-type aggregates in THF/H_2O mixtures.[28,30] Besides, light opalescence and a marked Tyndall effect were observed in THF/H_2O mixtures, which could further demonstrate the formation of nanoaggregates (Figure 2c). The dynamic light scattering (DLS) results revealed that the hydrodynamic diameters of the BBDP aggregates were not related to the concentration. The average size was calculated to be 1.2 μm (Figure S7).

Scanning electron microscopy (SEM) experiments were performed to investigate the morphologies of the BBDP supra-

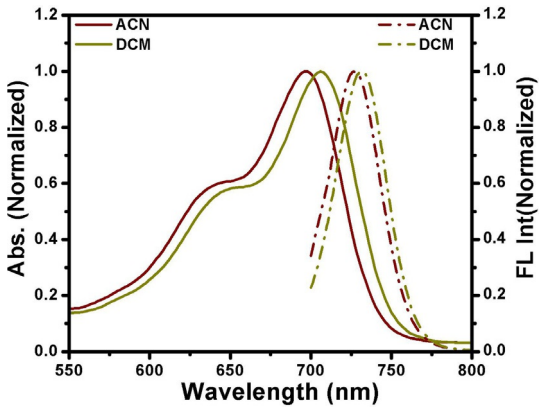

Figure 1. Normalized absorption and emission spectra of BBDP in different solvents ($c = 10$ μM). ACN = acetonitrile, DCM = dichloromethane.

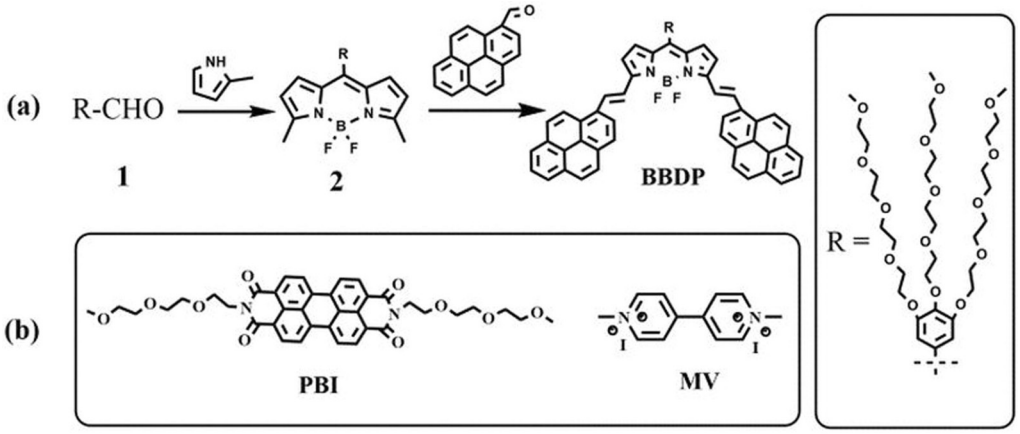

Scheme 1. a) Procedure for the synthesis of BBDP; b) structures of PBI and MV studied in the present work.

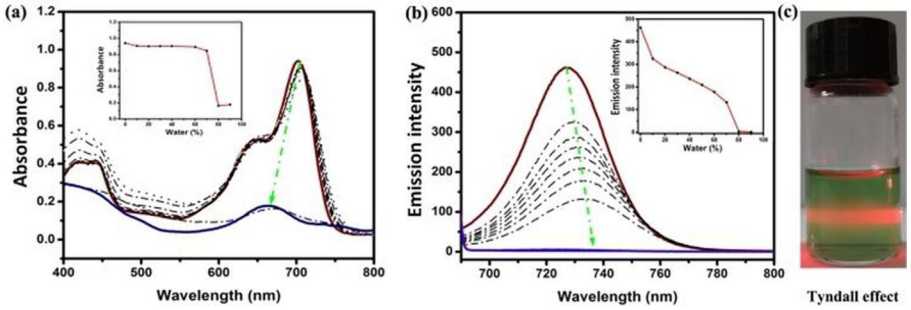

Figure 2. a) UV/Vis and b) fluorescence spectra of BBDP with different water fractions in THF/H_2O ($c = 10$ μM); c) Tyndall effect of BBDP assemblies in THF/H_2O ($c = 10$ μM).

molecular assemblies in aqueous solution (Figure 3 a–c). Interestingly, a great deal of wire-like nanostructures were observed for the aggregates in water media. In addition, these nanofibers possessed relatively high length/diameter ratios. The length of the nanofibers was up to several micrometers, and the diameter of the nanoassemblies was approximately several dozens of nanometers. An atomic force microscopy (AFM) image also revealed the existence of nanofibers on the mica surface (Figure 3 d). AFM image analysis was applied to collect the height information of the obtained nanofibers. As shown in Figure 3 e, the height of these nanofibers was measured to be approximately 40 nm, whereas the diameter of the nanowires was approximately 100 nm (Figure 3 e). To investigate the mechanism for the formation of the nanofiber morphology, we speculated that the hydrophilic OEG chains were exposed to highly polar water, whereas the planar hydrophobic moieties preferred to form H-type assemblies to minimize the free energy. In this way, the nanoaggregates presented a fiber-like morphology. Fluorescent microscopy images also revealed the existence of wire-like structures. Owing to the NIR properties of the BBDP aggregates, NIR-emissive nanofibers could be obtained from the fluorescent microscopy images (Figure S10).

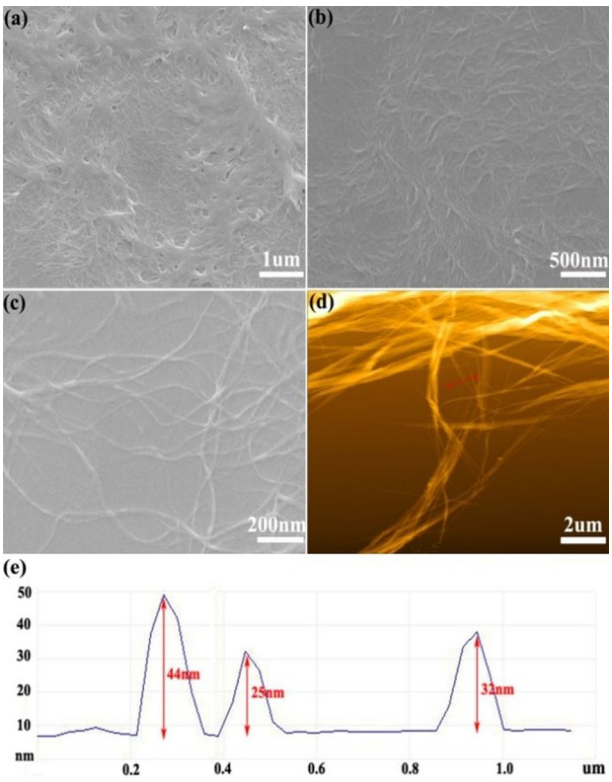

Figure 3. a–c) SEM images with different magnifications of BBDP aggregates in aqueous solution ($c = 6$ μM); d) AFM morphology image of BBDP aggregates in aqueous solution ($c = 4$ μM); e) section analysis of the nanoaggregates.

Charge-transfer interactions and aggregate morphology

NIR-emissive BBDP possesses the potential to co-assemble with electron-poor molecules by charge-transfer interaction as a result of the existence of the pyrene moieties. We noticed that the charge-transfer strategy might be a feasible way to manipulate the nanostructures of the NIR aggregates with high efficiency. In this regard, PBI and MV were selected as electron-deficient acceptor molecules, whereas BBDP behaved as an electron-rich donor molecule. As is well known, pyrene units can initially assemble with viologen or perylene bisimide groups with a molar ratio of 1:1 to form supramolecular complexes driven by charge-transfer interactions.[31,32,39,44,49] Considering that MV has stronger electron-withdrawing ability than PBI, we wondered whether any morphology variation would be achieved by adding different acceptor molecules.

The co-assembly behavior between BBDP and MV was investigated by ^{1}H NMR spectroscopy. The signals between $\delta = 8.9$ and 7.9 ppm were all ascribed to the pyrene units, whereas the resonances at $\delta = 7.46$ and 7.14 ppm were ascribed to the protons on the pyrrole rings of BBDP. After the addition of MV, a dramatic upfield shift in the signals in the low-field region was observed. As shown in Figure 4 a, the resonances of the protons on BBDP and MV (molar ratio of 1:2) showed upfield shifts owing to the formation of a charge-transfer complex. This phenomenon may be attributed to ring-current shielding effects induced by strong π–π interactions between BBDP and MV. This result is consistent with previous reports by other researchers.[32,39,40] The ^{1}H NMR spectrum of the BBDP–PBI complex was obtained in $CDCl_3$ solvent (Figure S1). The chemical shifts of the supramolecular complex follow the same trend in that the signals in the aromatic region are upfield shifted.

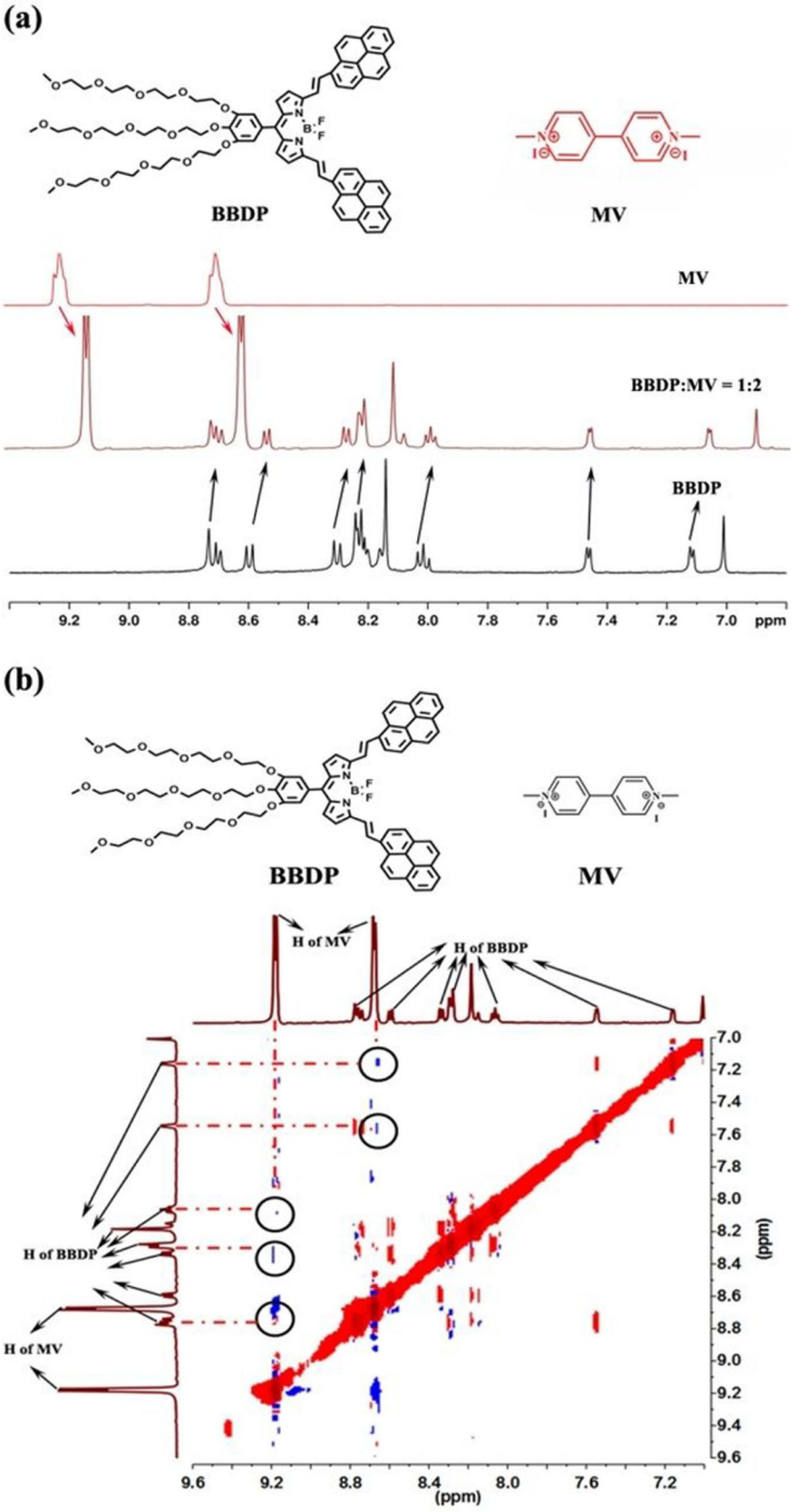

Figure 4. a) ^{1}H NMR spectra of BBDP ($c = 2$ mM), the BBDP–MV (molar ratio = 1:2, $c_{BBDP} = 2$ mM) co-assembly complex, and MV ($c = 2$ mM) in [D_8]THF/D_2O. b) 2D ^{1}H NMR NOESY spectrum of the BBDP–MV (molar ratio = 1:2, $c_{BBDP} = 2$ mM) complex in [D_8]THF/D_2O (5:1, *v*/*v*).

Thus, the ^{1}H NMR spectroscopy data provided direct evidence for the formation of charge-transfer complexes.

Nuclear Overhauser effect spectroscopy (NOESY) was exploited to elaborate the structure of the charge-transfer complex further. The distance between the donor and acceptor molecules would be shortened to less than 5 Å by the charge-transfer interaction.[39] Therefore, NOE signals could be observed upon the formation of the charge-transfer complex. The 2D ^{1}H NMR NOESY spectrum of the BBDP–PBI complex (molar ratio of 1:2) in $CDCl_3$ was collected. As shown in Figure S2, correlations between the protons of BBDP and PBI were observed, which is indicative of the formation of the supramolecular complex. MV is an electron-deficient group that has higher electron-withdrawing capacity than PBI. Upon mixing MV with BBDP in a molar ratio of 2:1 in [D_8]THF/D_2O, much stronger correlations were detected and more correlation spots were found in the 2D ^{1}H NMR spectrum (Figure 4b). This effect was mainly associated to change in the electron-withdrawing ability. UV/Vis and FL spectrometry were employed to obtain more photophysical information on the two charge-transfer complexes (Figures S3 and S4). Beyond our expectations, little change in the absorption spectra occurred, and the emission intensity of the obtained charge-transfer complex only showed a faint decrease. We propose that the BODIPY derivatives are stable fluorescent materials that obtain the capacity to withstand external factors. Hence, two novel charge-transfer complexes with NIR emission were realized by utilizing the charge-transfer strategy.

By utilizing photophysical methods, the aggregation behavior of the above two charge-transfer systems could be observed directly in a water environment. As for the BBDP–MV charge-transfer complex, the absorption band at approximately $\lambda = 700$ nm decreased in intensity upon increasing the water fraction (Figure S5). Moreover, the absorption intensity decreased dramatically, which was accompanied by a $\Delta\lambda = 40$ nm hypsochromic shift if the water ratio reached 80%. During the aggregation procedure, the emission intensity suffered a sharp decrease and was fully quenched in the end. Hence, it could be seen that the BBDP–MV complex formed H-type aggregates in aqueous media. By integrating with the PBI molecules through the charge-transfer noncovalent interaction, the BBDP–PBI complex possessed a higher hydrophobic ratio than BBDP alone. Thus, the BBDP–PBI complex might be more inclined to assemble at the same concentration. As shown in Figure S6, the absorption intensity began to drop upon the initial addition of water to the system. When the water fraction reached 70%, the absorption intensity decreased to almost half of the original intensity. Both the absorption and emission bands expressed marked bathochromic shifts, whereas the fluorescent emission was quenched after the addition of water. We speculate that H-type and J-type aggregation cooperate with each other in the system. The formation of nanoparticles was further confirmed by DLS measurements. The hydrodynamic diameter of the BBDP–MV ($c_{BBDP} = 6$ μM) aggregates was calculated to be 250 nm with a relatively low polydispersity index (PDI = 0.243) (Figure S8). The BBDP–PBI ($c_{BBDP} = 6$ μM) assemblies possessed a much larger aggregation size of approximately 667 nm (PDI = 0.212) (Figure S9). Furthermore, the hydrodynamic diameters of the BBDP–PBI aggregates were founded to increase upon increasing the concentration. However, the aggregate size showed little dependence on the concentration for the BBDP–MV system.

Considering the amphiphilic nature of the two as-prepared charge-transfer complexes, we speculate that novel NIR nanoaggregates can be realized in aqueous media. In an effort to elucidate the architecture of the resulting nanoassembly, SEM and AFM imaging were performed at multiple locations across the samples. As we expected, the BBDP–PBI superamphiphile self-assembly displays a typical nanorod suprastructure, as seen by SEM (Figure 5a, b). These nanorods have an external diameter of approximately 50 nm and are up to more than 1 μm in length. AFM characterization also demonstrates the formation of rod-like structures, which is consistent with the SEM results (Figure 5c). This observation should be attributed

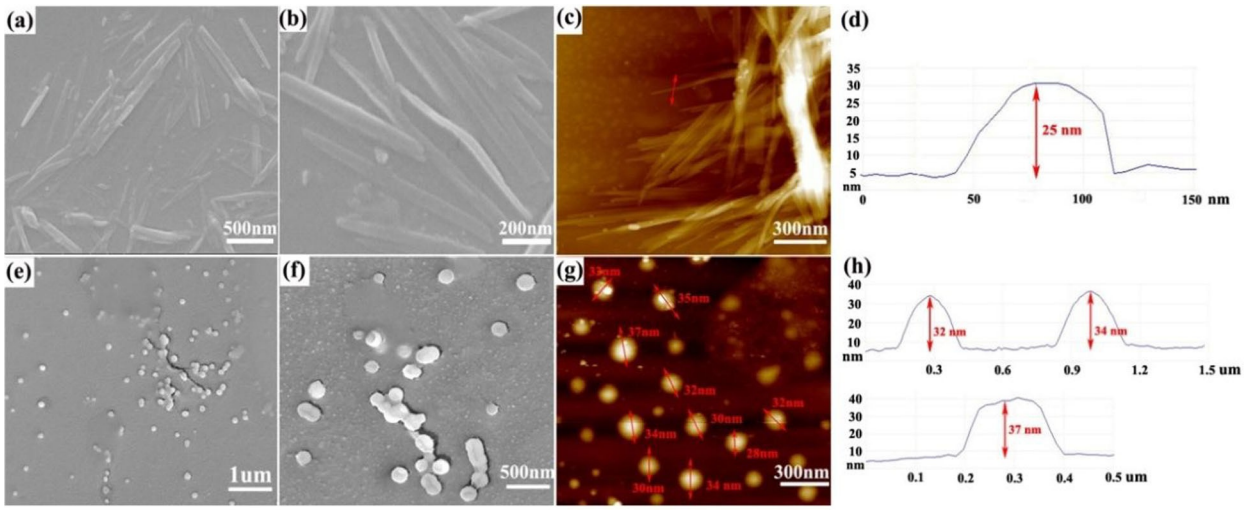

Figure 5. a, b) SEM images and c, d) AFM images with individual heights of the BBDP–PBI nanoaggregates (molar ratio = 1:2, $c_{BBDP} = 6$ μM) in THF/H_2O; e, f) SEM images and g, h) AFM images with individual heights of the BBDP–MV nanoaggregates (molar ratio = 1:2, $c_{BBDP} = 6$ μM) in THF/H_2O.

to the monolayer arrangement of the BBDP–PBI charge-transfer complex. To investigate the morphology further, nanoscopy analysis software was employed to collect more information on the aggregates. The height of the nanorods was found to be approximately 25 nm, and the lateral size of the nanorods is approximately 80 nm, which is in accordance with the SEM results above (Figure 5d). In contrast, the BBDP–MV complex nanoassembly shows a different morphology. Numerous nanodisks with uniform size are detected in the SEM images (Figure 5e,f). The lateral size of the nanoaggregates is approximately 200 nm. Similar nanostructures are obtained from the AFM results, which further confirms the generation of nanodisks. AFM height analysis reveals that these nanodisks possess a rather uniform height. These nanodisks have an average height of 34 nm, whereas the diameter of the nanodisks is approximately 200 nm (Figure 5g,h). As indicated by fluorescent microscopy images, the BBDP–MV aggregates have a nanodisk morphology and present red emission under excitation with specific wavelength light, whereas BBDP–PBI self-assembles into nanorods (Figures S11 and S12).

With the different self-assembly morphologies in hand, a model was proposed (Scheme 2). BBDP possesses large planar rigid structures underneath and flexible OEG chains on top. The hydrophobic planar blocks are inclined to assemble to generate the core of the nanofibers, and the hydrophilic OEG chains are exposed to the exterior water environment. Hence, a fiber-like morphology can be obtained, as observed in the SEM and AFM images. After the formation of charge-transfer co-assembly complexes, the self-assembly behavior is different so that the nanoaggregates present distinct morphologies. As for the BBDP–PBI superamphiphile, two PBI units are attached to BBDP owing to the existence of a charge-transfer interaction. In this way, the obtained superamphiphile possesses two hydrophilic parts. Different from the aggregation behavior of BBDP, the two hydrophilic parts at both ends of the BBDP–PBI superamphiphile tend to remain bare in water media, whereas the hydrophobic parts pile together to promote water solubility. Then, the nanorods can eventually be formed. The BBDP–MV superamphiphile has an architecture that is similar to that of the BBDP–PBI complex. The distinct morphology of the nanoaggregates may be associated with better water solubility or the smaller size of the MV groups.

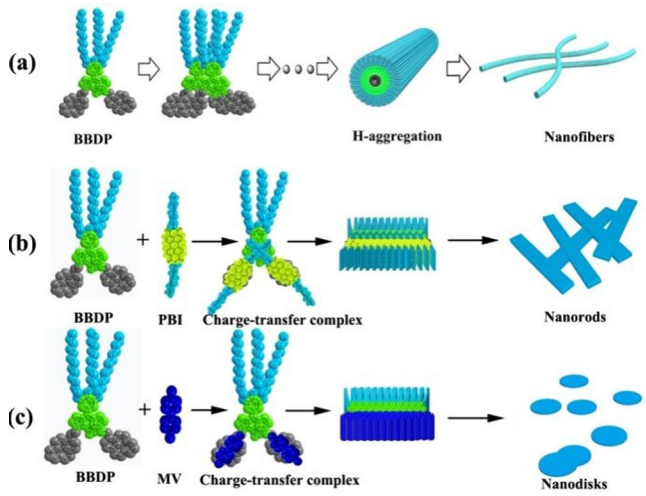

Scheme 2. Schematic illustrations for the formation of a) nanofibers from BBDP, b) nanorods from the co-assembly of BBDP and PBI, and c) nanodisk aggregates from the co-assembly of BBDP and MV.

Conclusions

In summary, a novel near-infrared (NIR)-emissive boron–dipyrromethene (BODIPY) derivative, BBDP, was prepared. This amphiphilic structure was shown to have the potential to self-assemble in aqueous solution. By utilizing the charge-transfer interactions, BBDP was transformed into two novel superamphiphiles that could form nanoaggregates in aqueous media. BBDP alone could self-assemble into nanofibers, whereas the BBDP–PBI (PBI = perylene bisimide derivative) complex aggregated to form a nanorod morphology. Furthermore, numerous nanodisks with uniform size were observed in the scanning electron microscopy and atomic force microscopy images of the assemblies of the BBDP–MV (MV = viologen derivative) complex. Therefore, morphology transition could be achieved by introducing a charge-transfer interaction. Considering the NIR properties of the three nanoassemblies, these NIR materials might show potential applications in many fields. Through integration with specific functional groups by charge-transfer interactions, specific applications were able to be achieved. Further work on this aspect to design functional materials based on NIR BODIPY derivatives is ongoing in our laboratory.

Experimental Section

Materials

All reagents were purchased from commercial sources and were used without further purification unless otherwise stated. Solvents were dried by fluxing under nitrogen with calcium hydroxide. All the reactions stated in this paper were performed in dried glassware under a nitrogen atmosphere. Analytical thin-layer chromatography (TLC) was performed on precoated silica-gel plates (0.4–0.5 mm thick). Column chromatography was performed on silica gel (200–300 mesh) as the stationary phase. Deionized water was obtained from an ultrapure water system (HITRCH Smaret-S15).

Instruments and measurements

^{1}H NMR and ^{13}C NMR spectra were recorded with a Bruker Avance spectrometer at 400 and 100 MHz, respectively, at 298 K. All chemical shifts are reported in parts per million (ppm) by using tetramethylsilane as an internal reference. A Hitachi U-5100 spectrometer was used to measure the UV/Vis absorption spectra. Fluorescence emission spectra were recorded with a Hitachi F-2700 spectrometer. High-resolution mass spectrometry experiments were performed with a Bruker Daltonics Apex IV spectrometer. SEM images were obtained with a JSM 6390LV microscope. AFM experiments were performed with a Bruker Nanoscope VIII Multimode microscope. The sample was prepared by pipetting an aliquot of the corresponding solution on the mica surface and drying at room temperature. Nanoscope analysis software was exploited to investigate the AFM images. Fluorescent microscopy images were ob-

tained by using an OLYMPUS IX83 fluorescent microscope. The hydrodynamic diameters of the nanoaggregates at different concentrations were determined at 298 K with a ZEN3600 MALVERN by dynamic light scattering (DLS). X-ray diffraction (XRD) patterns of the samples were measured with an Advance D8.

Construction of amphiphilic assemblies

Preparation of BBDP aggregates: BBDP was dissolved in tetrahydrofuran to form a solution with a concentration of 2.4×10^{-5} mol L^{-1}. Deionized water (3 mL) was added dropwise into the above BBDP solution (1 mL) to induce aggregate formation accompanied by stirring at a relatively low speed of 200 rpm. The mixture was stirred for 2 h and was then left to stand for 12 h.

Preparation of BBDP–PBI aggregates: The sample was prepared in the same manner as that described above except the initial tetrahydrofuran solution consisted of BBDP/PBI = 1:2 with a BBDP concentration of 2.4×10^{-5} mol L^{-1}.

Preparation of BBDP–MV aggregates: The sample was prepared in the same manner as that described above except the initial tetrahydrofuran solution consisted of BBDP/MV = 1:2 with a BBDP concentration of 2.4×10^{-5} mol L^{-1}.

Synthesis and characterization

2: Compound **1** was synthesized according to the literature.[45] Compound **1** (700 mg, 0.97 mmol) and 2-methylpyrrole (162 mg, 2.0 mmol) were dissolved in anhydrous CH_2Cl_2 (150 mL). Trifluoroacetic acid (TFA, 2 drops) was added to the mixture as the catalyst. The reaction was performed at room temperature with stirring for 12 h under a nitrogen atmosphere. Then, 2,3-dicyano-5,6-dichlorobenzoquinone (DDQ; 220 mg, 0.97 mmol) was added to the system, which was stirred for another 12 h. *N*,*N*-Diisopropylethylamine (DIEA, 2 mL) was added with ice bathing for 10 min. $BF_3{\cdot}OEt_2$ (4 mL) was added to the mixture, which was stirred for 8 h. After the reaction was over, the solvent was evaporated under reduced pressure. The crude product was purified by chromatography (silica gel, CH_2Cl_2/CH_3OH = 20:1, *v*/*v*) to afford **2** (300 mg, 34%). ^{1}H NMR (400 MHz, $CDCl_3$): δ = 6.78 (d, *J* = 4.0 Hz, 2H), 6.74 (s, 2H), 6.26 (d, *J* = 4.0 Hz, 2H), 4.23 (t, *J* = 4.8 Hz, 2H), 4.15 (t, *J* = 4.8 Hz, 4H), 3.52–3.81 (m, 42H), 3.36 (d, *J* = 6.9 Hz, 9H), 2.63 ppm (s, 6H). ^{13}C NMR (100 MHz, $CDCl_3$): δ = 156.85, 151.87, 139.61, 133.73, 129.96, 128.70, 118.99, 109.96, 72.12, 71.46, 70.34, 70.20, 70.14, 70.02, 69.28, 68.70, 58.52 ppm. MS (ESI): *m*/*z*: calcd for $C_{44}H_{69}BF_2N_2O_{15}K$: 953.4396 [*M*+K$^+$]; found: 953.4852.

BBDP:[26] Compound **2** (100 mg, 0.11 mmol), 1-pyrenecarboxaldehyde (100 mg, 0.44 mmol), and *p*-toluenesulfonic acid (*p*-TsOH, 10 mg) were dissolved in a mixture of toluene (25 mL) and piperidine (1 mL). The mixture was stirred at 120 °C for 2 h under the protection of N_2. After that, the temperature was increased to 150 °C, and the solvent was evaporated into a Dean–Stark apparatus. Then, toluene (25 mL) and piperidine (1 mL) were added to the system, and the dryness process was repeated (6×) until the reagent was consumed. The crude product was washed with water, dried with $MgSO_4$, filtered, and concentrated. The residue was subjected to column chromatography (CH_2Cl_2/CH_3OH = 10:1, *v*/*v*) to afford a dark-green solid (40 mg, 27%). ^{1}H NMR (400 MHz, $CDCl_3$): δ = 8.63–8.51 (m, 6H), 8.26–8.03 (m, 22H), 7.21 (d, *J* = 4.6 Hz, 2H), 7.01 (d, *J* = 4.4 Hz, 2H), 6.87 (s, 2H), 4.30 (t, *J* = 5.2 Hz, 2H), 4.24 (t, *J* = 5.0 Hz, 4H), 3.91–3.53 (m, 42H), 3.35 ppm (d, *J* = 12.2 Hz, 9H). ^{13}C NMR (100 MHz, $CDCl_3$): δ = 154.92, 152.60, 140.12, 138.73, 136.53, 133.01, 132.07, 131.55, 130.89, 130.52, 129.75, 129.08, 128.20, 127.66, 125.88, 125.50, 125.11, 124.89, 122.52, 116.85, 110.62, 72.70, 72.04, 70.97, 70.76, 70.60, 69.86, 69.26, 59.12 ppm. MS (ESI): *m*/*z*: calcd for $C_{78}H_{85}BF_2N_2O_{15}K$; 1377.5648 [*M*+K$^+$]; found: 1377.6412.

PBI:[46] 3,4,9,10-Perylenetetracarboxylic dianhydride (1.00 mmol, 0.39 g) and 2-[2-(2-methoxyethoxy)ethoxy]ethylamine (2.50 mmol, 0.40 g) were placed in an oven-dried, three-necked flask. Imidazole (44.1 mmol, 3 g) and a catalytic amount of $Zn(OAc)_2$ were added to the system. The mixture was heated to 160 °C and stirred for 18 h under the protection of N_2. After the reaction mixture was cooled down to room temperature, deionized water (100 mL) was added, and the mixture was stirred for 20 min and 5% HCl was used to remove residual imidazole. Then, the mixture was extracted with CH_2Cl_2 and the organic layer was collected. The organic layer was dried with $MgSO_4$. The solvent was evaporated under reduced pressure. The crude product was purified by column chromatography (CH_2Cl_2/CH_3OH = 20:1, *v*/*v*) to afford a red-brown solid (320 mg, 47%). ^{1}H NMR (400 MHz, $CDCl_3$): δ = 3.32 (s, 6H), 3.46–3.49 (m, 4H), 3.59–3.62 (m, 4H), 3.64–3.66 (m, 4H), 3.74–3.76 (m, 4H), 3.87 (t, *J* = 6.00 Hz, 4H), 8.45 (d, *J* = 8.08 Hz, 4H), 8.56 ppm (d, *J* = 7.96 Hz, 4H).

MV:[47] 4,4′-Bipyridine (100 mg, 0.64 mmol) and an excess amount of iodomethane (4.0 g, 28 mmol) were dissolved in anhydrous acetonitrile (20 mL). The mixture was heated to 80 °C and stirred for 20 h under a N_2 atmosphere. After cooling down to room temperature, the solvent was evaporated under reduced pressure. The residue was dried in a vacuum drying oven to remove residual iodomethane, and the resulting product was obtained as a red powder (270 mg, 96%). ^{1}H NMR (400 MHz, D_2O): δ = 4.51 (s, 6H), 8.53 (d, *J* = 6.26 Hz, 4H), 9.06 ppm (d, *J* = 6.32 Hz, 4H).

Acknowledgements

This work was supported by the State Key Laboratory of Powder Metallurgy, Central South University, and the National Natural Science Foundation of China (NSFC No. 21204047).

Conflict of interest

The authors declare no conflict of interest.

Keywords: amphiphiles · charge transfer · morphology transition · nanostructures · self-assembly

[1] M. Vybornyi, A. V. Rudnev, S. M. Langenegger, T. Wandlowski, G. Calzaferri, R. Haner, *Angew. Chem. Int. Ed.* **2013**, *52*, 11488–11493; *Angew. Chem.* **2013**, *125*, 11702–11707.
[2] T. Fukui, S. Kawai, S. Fujinuma, Y. Matsushita, T. Yasuda, T. Sakurai, S. Seki, M. Takeuchi, K. Sugiyasu, *Nat. Chem.* **2017**, *9*, 493–499.
[3] X. Zhang, S. Rehm, M. M. Safont-Sempere, F. Würthner, *Nat. Chem.* **2009**, *1*, 623–629.
[4] T. Shimizu, M. Masuda, H. Minamikawa, *Chem. Rev.* **2005**, *105*, 1401–1443.
[5] Y. Kim, S. Shin, T. Kim, D. Lee, C. Seok, M. Lee, *Angew. Chem. Int. Ed.* **2013**, *52*, 6426–6429; *Angew. Chem.* **2013**, *125*, 6554–6557.
[6] S. S. Babu, V. K. Praveen, A. Ajayaghosh, *Chem. Rev.* **2014**, *114*, 1973–2129.
[7] R. D. Mukhopadhyay, V. K. Praveen, A. Ajayaghosh, *Sci. Rep.* **2015**, *5*, 09842.
[8] S. Ghosh, V. K. Praveen, A. Ajayaghosh, *Annu. Rev. Mater. Res.* **2016**, *46*, 235–262.
[9] S. Ghosh, D. S. Philips, A. Saeki, A. Ajayaghosh, *Adv. Mater.* **2017**, *29*, 1605408.

[10] X. Zhang, D. Gorl, V. Stepanenko, F. Würthner, *Angew. Chem. Int. Ed.* **2014**, *53*, 1270 – 1274; *Angew. Chem.* **2014**, *126*, 1294 – 1298.
[11] A. Barbieri, E. Bandini, F. Monti, V. K. Praveen, N. Armaroli, *Top. Curr. Chem.* **2016**, *374*, 47.
[12] S. Cherumukkil, S. Ghosh, P. V. Karthikeyan, A. Ajayaghosh, *Chem. Sci.* **2017**, *8*, 5644 – 5649.
[13] P. Anees, S. Sreejith, A. Ajayaghosh, *J. Am. Chem. Soc.* **2014**, *136*, 13233 – 13239.
[14] V. J. Pansare, S. Hejazi, W. J. Faenza, R. K. Prud'homme, *Chem. Mater.* **2012**, *24*, 812 – 827.
[15] N. Boens, V. Leen, W. Dehaen, *Chem. Soc. Rev.* **2012**, *41*, 1130 – 1172.
[16] A. Loudet, K. Burgess, *Chem. Rev.* **2007**, *107*, 4891 – 4932.
[17] G. Ulrich, R. Ziessel, A. Harriman, *Angew. Chem. Int. Ed.* **2008**, *47*, 1184 – 1201; *Angew. Chem.* **2008**, *120*, 1202 – 1219.
[18] P. P. Goswami, A. Syed, C. L. Beck, T. R. Albright, K. M. Mahoney, R. Unash, E. A. Smith, A. H. Winter, *J. Am. Chem. Soc.* **2015**, *137*, 3783 – 3786.
[19] L. J. Jiao, Y. Y. Wu, Y. Ding, S. F. Wang, P. Zhang, C. J. Yu, Y. Wei, X. L. Mu, E. H. Hao, *Chem. Asian J.* **2014**, *9*, 805 – 810.
[20] H. Sunahara, Y. Urano, H. Kojima, T. Nagano, *J. Am. Chem. Soc.* **2007**, *129*, 5597 – 5604.
[21] C. J. Yu, L. J. Jiao, T. T. Li, Q. H. Wu, W. Miao, J. Wang, Y. Wei, X. L. Mu, E. H. Hao, *Chem.Commun.* **2015**, *51*, 16852 – 16855.
[22] J.-F. Yin, Y. Hu, D.-G. Wang, L. Yang, Z. Jin, Y. Zhang, G.-C. Kuang, *ACS Macro Lett.* **2017**, *6*, 139 – 143.
[23] H. Lu, J. Mack, Y. C. Yang, Z. Shen, *Chem. Soc. Rev.* **2014**, *43*, 4778 – 4823.
[24] W. L. Zhao, E. M. Carreira, *Angew. Chem. Int. Ed.* **2005**, *44*, 1677 – 1679; *Angew. Chem.* **2005**, *117*, 1705 – 1707.
[25] C. J. Jiao, N. N. Zu, K. W. Huang, P. Wang, J. S. Wu, *Org. Lett.* **2011**, *13*, 3652 – 3655.
[26] L. Yang, Y. J. Ji, J.-F. Yin, Y. Q. Wu, H. M. Fan, Y. Zhang, G.-C. Kuang, *Soft Matter* **2016**, *12*, 8581 – 8587.
[27] H. He, S. S. Ji, Y. He, A. J. Zhu, Y. L. Zou, Y. B. Deng, H. T. Ke, H. Yang, Y. L. Zhao, Z. Q. Guo, H. B. Chen, *Adv. Mater.* **2017**, *29*, 1606690.
[28] Z. Q. Guo, Y. L. Zou, H. He, J. M. Rao, S. S. Ji, X. N. Cui, H. T. Ke, Y. B. Deng, H. Yang, C. Y. Chen, Y. L. Zhao, H. B. Chen, *Adv. Mater.* **2016**, *28*, 10155 – 10164.
[29] L. Quan, S. Liu, T. T. Sun, X. G. Guan, W. H. Lin, Z. G. Xie, Y. Huang, Y. Q. Wang, X. B. Jing, *ACS Appl. Mater. Interfaces* **2014**, *6*, 16166 – 16173.
[30] Z. J. Chen, Y. Liu, W. Wagner, V. Stepanenko, X. K. Ren, S. Ogi, S. F. Würthner, *Angew. Chem. Int. Ed.* **2017**, *56*, 5729 – 5733; *Angew. Chem.* **2017**, *129*, 5823 – 5827.
[31] A. Das, S. Ghosh, *Angew. Chem. Int. Ed.* **2014**, *53*, 2038 – 2054; *Angew. Chem.* **2014**, *126*, 2068 – 2084.
[32] W. Yu, X. Y. Wang, J. Li, Z. T. Li, Y. K. Yan, W. Wang, J. Pei, *Chem. Commun.* **2013**, *49*, 54 – 56.
[33] M. Kumar, K. V. Rao, S. J. George, *Phys. Chem. Chem. Phys.* **2014**, *16*, 1300 – 1313.
[34] Y. Li, W. Wang, W. R. Leow, B. Zhu, F. Meng, L. Zheng, J. Zhu, X. Chen, *Small* **2014**, *10*, 2776 – 2781.
[35] A. Das, S. Ghosh, *Angew. Chem. Int. Ed.* **2014**, *53*, 1092 – 1097; *Angew. Chem.* **2014**, *126*, 1110 – 1115.
[36] C. Wang, X. Zhang, *Chem. Soc. Rev.* **2011**, *40*, 94 – 101.
[37] H. J. Kim, J. Heo, W. S. Jeon, E. Lee, J. Kim, S. Sakamoto, K. Yamaguchi, K. Kim, *Angew. Chem. Int. Ed.* **2001**, *40*, 1526 – 1529; *Angew. Chem.* **2001**, *113*, 1574 – 1577.
[38] C. Wang, S. C. Yin, S. L. Chen, H. P. Xu, Z. Q. Wang, X. Zhang, *Angew. Chem. Int. Ed.* **2008**, *47*, 9049 – 9052; *Angew. Chem.* **2008**, *120*, 9189 – 9192.
[39] C. Wang, Y. S. Guo, Y. P. Wang, H. P. Xu, R. J. Wang, X. Zhang, *Angew. Chem. Int. Ed.* **2009**, *48*, 8962 – 8965; *Angew. Chem.* **2009**, *121*, 9124 – 9127.
[40] K. Liu, Y. X. Yao, Y. Liu, C. Wang, Z. B. Li, X. Zhang, *Langmuir* **2012**, *28*, 10697 – 10702.
[41] K. Liu, Y. X. Yao, C. Wang, Y. Liu, Z. B. Li, X. Zhang, *Chem. Eur. J.* **2012**, *18*, 8622 – 8628.
[42] K. Liu, C. Wang, Z. B. Li, X. Zhang, *Angew. Chem. Int. Ed.* **2011**, *50*, 4952 – 4956; *Angew. Chem.* **2011**, *123*, 5054 – 5058.
[43] Y. L. Liu, Y. Yu, J. A. Gao, Z. Q. Wang, X. Zhang, *Angew. Chem. Int. Ed.* **2010**, *49*, 6576 – 6579; *Angew. Chem.* **2010**, *122*, 6726 – 6729.
[44] C. Wang, Y. Guo, Y. Wang, H. Xu, X. Zhang, *Chem. Commun.* **2009**, 5380 – 5382.
[45] H. Wang, Y. Q. Wu, P. Tao, X. Fan, G.-C. Kuang, *Chem. Eur. J.* **2014**, *20*, 16634 – 16643.
[46] R. Samudrala, X. Zhang, R. M. Wadkins, D. L. Mattern, *Bioorg. Med. Chem.* **2007**, *15*, 186 – 193.
[47] S. Datta, N. Dey, S. Bhattacharya, *Chem. Commun.* **2017**, *53*, 2371 – 2374.
[48] S. N. You, K. L. Zhong, L. Y. Jin, *Soft Matter* **2017**, *13*, 3334 – 3340.
[49] K. Wang, Z. X. Guo, L. Zhang, K. Sun, P. Yu, S. H. Zhou, W. P. Wang, Z. B. Li, *Soft Matter* **2017**, *13*, 1948 – 1955.

Manuscript received: September 11, 2017
Accepted manuscript online: September 27, 2017
Version of record online: November 3, 2017